INTERNATIONAL JOURNAL FOR NUMERICAL AND ANALYTICAL METHODS IN GEOMECHANICS, VOL. 18, 177–203 (1994)

ANALYSIS OF FULLY COUPLED THERMOMECHANICAL BEHAVIOUR AROUND A RIGID CYLINDRICAL HEAT SOURCE BURIED IN CLAY

H. N. SENEVIRATNE

Department of Civil Engineering, University of Peradeniya, Peradeniya, Sri Lanka

J. P. CARTER AND J. R. BOOKER

School of Civil and Mining Engineering, The University of Sydney, NSW 2006, Australia

SUMMARY

The problem of fully coupled consolidation and heat flow around a rigid cylindrical heat source buried in clay has been studied. The governing equations of the problem are summarized in the paper and a finite element time-marching scheme to obtain an approximate solution to the governing equations is described. The stress–strain behaviour of the skeleton of the saturated soil has been represented by both a linear elastic model and the modified Cam clay soil model. The results of a limited parametric study are presented with the aim of understanding the major mechanisms of soil behaviour close to buried canisters of hot radioactive waste. A range of soil properties has been included in the study, and the effects of soil disturbance during canister emplacement have also been considered.

1. INTRODUCTION

The problem of heat flow and consolidation around heat sources buried in clay has generated considerable research interest recently. This is due particularly to the encounter of such behaviour in the disposal of radioactive waste. In some proposed disposal methods metal canisters of vitrified radioactive waste are to be buried in the seabed or in deep formations of clay of low permeability. In the multi-barrier system,[1] the canister forms the first barrier, but in the long time scale considered, the soil surrounding the canister provides the long-term protection against contamination. In this case the canister acts as a heat source after emplacement, although its power diminishes gradually with radioactive decay. Obviously, the thermomechanical behaviour of the soil surrounding the canister is of great importance in assessing its effectiveness as a barrier. The excess pore pressures generated due to heat transfer may cause water to flow away from the canister, thus increasing the area of potential contamination. Furthermore, the generation of high excess pore pressures could ultimately result in hydrofracture of the soil. Fractures of this type can occur in the soil close to the canister, seriously compromising the effectiveness of the soil as a long-term barrier. It is also important to assess reliably the effect of disturbance created during the emplacement of the canister on the subsequent thermomechanical bahaviour.

This paper describes finite element analyses carried out of the fully coupled consolidation and heat flow around a rigid cylindrical heat source buried in clay. The canister is assumed to be of sufficient length so that it can be considered as an infinitely long heat source. The stress–strain models for soil employed in the analyses are the linear elastic model and a version of the modified

CCC 0363–9061/94/030177–27

Received 7 May 1993
Revised 11 October 1993

Cam clay model, with incorporated thermal behaviour. The analyses were aimed at understanding the mechanisms of soil behaviour close to the canister and the influence on this behaviour of various soil parameters and the disturbance during canister emplacement. Realistic values have been assumed for soil properties although no attempt has been made to model a specific field problem.

2. LITERATURE REVIEW

Hickox and Watts[2] and Wickens[3] have reported the results of numerical analyses of heat flow and pore pressure dissipation around a decaying cylindrical heat source in a rigid porous medium. Their analyses have demonstrated that the temperature drops sharply away from the heat source. The differential thermal expansion between pore water and soil particles was found to be the dominant factor in determining the pore pressure field. However, the contribution from soil compressibility has not been considered in calculating the pore pressures in the above analyses.

Booker and Savvidou[4] presented a semi-coupled solution for consolidation around a spherical heat source buried in a poroelastic medium using the Laplace transform techniques. The semi-coupled theory neglects the contribution from mechanical terms to the heat equation, which is generally considered insignificant for most practical cases. Their results indicated that the generation of excess pore pressures and the reduction of effective stresses are relatively small in more permeable soils. However, a major reduction in effective stress takes place in the radial direction close to the heat source. Smith[5] presented the fully coupled solution for the heat flow and consolidation around an infinitely long cylindrical heat source buried in an elastic soil. The distributions of temperature and pore pressure are somewhat similar to those given by Booker and Savvidou for the spherical source, but the rate of dissipation is much slower than in the spherical case due to the infinite extent of the cylindrical source. An interesting aspect of both the above solutions is that the rigidity of the heat source has no influence on the behaviour of the surrounding soil.

Lewis *et al.*[6] presented a fully coupled finite element formulation of consolidation of non-isothermal elastoplastic media. They obtained good agreement between their finite element results for the problem of thermoelastic consolidation around a cylindrical heat source and the approximate analytical solution for the same problem given by Booker and Savvidou.[4] Independently, Britto *et al.*[7] presented a fully coupled finite element formulation of heat transfer and consolidation behaviour. Britto *et al.*[8] also presented comparisons between the observed behaviour in the centrifuge of a heated cylindrical canister embedded in clay and the finite element predictions made using the modified Cam clay stress–strain model. In all cases they found good agreement between the observed and predicted temperatures. Good agreement was also found between the observed and predicted pore pressures in normally consolidated soil but not in overconsolidated soil.

Finite element analyses of fully coupled thermal consolidation around canisters have also been carried out by a research group at ISMES in Bergamo, Italy. For example, Heuckel *et al.*[9] presented a set of constitutive equations for the fully coupled thermoelastoplastic behaviour of a clay and also reported the finite element results of consolidation behaviour around a heated canister buried in clay. They concluded that thermal plastic yielding is beneficial in reducing the peak pore pressures around the canister, but also causes a large reduction in shear strength in the soil close to the canister.

3. GOVERNING EQUATIONS AND FINITE ELEMENT FORMULATION

The derivation given below is similar to that used by Britto *et al.*[7] for the fully coupled finite element formulation, but unlike the latter the symmetry of the governing equations is ensured.

3.1. Equilibrium

Let $\boldsymbol{\sigma}$ be the vector of stress increments of a body due to the applied loading and temperature change. $\boldsymbol{\sigma}$ is defined here with the usual geomechanics convention of compression positive. In the absence of body forces, equilibrium of the body can be expressed in a Cartesian co-ordinate system as

$$\partial^{\mathrm{T}}\boldsymbol{\sigma} = 0 \tag{1}$$

where $\boldsymbol{\sigma} = (\sigma_x, \sigma_y, \sigma_z, \tau_{xy}, \tau_{yz}, \tau_{zx})^{\mathrm{T}}$ and

$$\partial^{\mathrm{T}} = \begin{bmatrix} \partial/\partial x & 0 & 0 & \partial/\partial y & 0 & \partial/\partial z \\ 0 & \partial/\partial y & 0 & \partial/\partial x & \partial/\partial z & 0 \\ 0 & 0 & \partial/\partial z & 0 & \partial/\partial y & \partial/\partial x \end{bmatrix}$$

3.2. Strain–displacement relations

Using the geomechanics convention of positive compressive strains, these relations in matrix form are given by

$$\boldsymbol{\varepsilon} = -\partial\mathbf{u} \tag{2}$$

where $\boldsymbol{\varepsilon} = (\varepsilon_x, \varepsilon_y, \varepsilon_z, \gamma_{xy}, \gamma_{yz}, \gamma_{zx})^{\mathrm{T}}$ is the vector of strain components and $\mathbf{u} = (u_x, u_y, u_z)^{\mathrm{T}}$ is the vector of displacement components.

3.3. Principle of effective stress

There is no evidence to indicate that the principle of effective stress is affected by temperature changes. Hence it is convenient to use

$$\boldsymbol{\sigma} = \boldsymbol{\sigma}' + \mathbf{a}p \tag{3}$$

where $\boldsymbol{\sigma}' = (\sigma'_x, \sigma'_y, \sigma'_z, \tau_{xy}, \tau_{yz}, \tau_{zx})^{\mathrm{T}}$, $\mathbf{a} = (1, 1, 1, 0, 0, 0)^{\mathrm{T}}$ and p is the pore water pressure (a scalar quantity).

3.4. Constitutive relationship

In the absence of thermal effects the rate form of the stress–strain relationship may be expressed as

$$\dot{\boldsymbol{\sigma}}' = \mathbf{D}\dot{\boldsymbol{\varepsilon}} \tag{4a}$$

where the superior dot indicates a rate. $\mathbf{D}$ is a matrix of material parameters which for a linear

isotropic elastic material is given by

$$\mathbf{D} = \begin{bmatrix} \lambda + 2G & \lambda & \lambda & 0 & 0 & 0 \\ \lambda & \lambda + 2G & \lambda & 0 & 0 & 0 \\ \lambda & \lambda & \lambda + 2G & 0 & 0 & 0 \\ 0 & 0 & 0 & G & 0 & 0 \\ 0 & 0 & 0 & 0 & G & 0 \\ 0 & 0 & 0 & 0 & 0 & G \end{bmatrix}$$

where λ and G are Lamé constants. The derivation of $\mathbf{D}$ for the modified Cam clay model has been described in detail elsewhere, e.g. Reference 10.

In the presence of temperature changes equation (4a) may be expressed as

$$\dot{\boldsymbol{\sigma}}' = K'\beta\dot{\theta}\mathbf{a} + \mathbf{D}\dot{\boldsymbol{\varepsilon}} \tag{4b}$$

where θ is the temperature increase. K' is the effective bulk modulus of the soil given by

$$K' = \frac{1}{\mathbf{a}^{\mathrm{T}}\mathbf{D}^{-1}\mathbf{a}} \tag{5}$$

β is the coefficient of effective thermal volume expansion of the soil. Usually β is negative as an increase in the temperature causes a volumetric compression. It is implicitly assumed in deriving equation (5) that the stress changes induced by temperature changes, but not necessarily the thermal strains, are isotropic. There is no experimental evidence either to support or to contradict this assumption. However, the advantage here is that a displacement finite element formulation with the modified Cam clay model gives rise to a symmetric stiffness matrix, unlike the case where isotropic thermal strains are assumed.

3.5. Continuity condition

Assuming that the pore water and soil grains are incompressible, the continuity condition can be expressed as

$$\int_0^t \nabla^{\mathrm{T}}\mathbf{v} = \varepsilon_v + \alpha\theta \tag{6}$$

where $\nabla^{\mathrm{T}} = (\partial/\partial x, \partial/\partial y, \partial/\partial z)$ is the gradient operator, $\mathbf{v} = (v_x, v_y, v_z)^{\mathrm{T}}$ is the seepage velocity, $\varepsilon_v = \mathbf{a}^{\mathrm{T}}\boldsymbol{\varepsilon}$ is the volumetric strain, $\alpha = (1 - n)\alpha_s + n\alpha_w$ is the coefficient of undrained thermal volume expansion, and n is the porosity of the soil. Under undrained conditions, there is no seepage water flow throughout the soil, i.e. the left-hand side of equation (6) equals zero. Under fully drained conditions there is no generation of excess pore pressure anywhere.

It is important to distinguish clearly between the meanings of the soil parameters α and β introduced above. As mentioned previously, α is the coefficient of undrained thermal expansion and it describes the overall expansion of both the solid particles and the pore fluid within a soil element that occurs purely as a result of a temperature change. On the other hand, β, which is the coefficient of effective thermal volume expansion, describes the volume change of a soil element associated purely with flow of the pore fluid and hence the dissipation of positive pore pressures generated originally by heating of the soil.

3.6. *Conservation of energy*

The complete coupling of mechanical and thermal processes has been investigated by several researchers using different methods. The equation adopted here has been derived by Smith.[5] Convection terms are not included in this derivation as Hickox and Watts[2] have shown that they can be safely ignored in relatively impermeable clayey soils. Consequently, for linear material behaviour, the conservation of energy is described by

$$\int_0^t -\nabla^{\mathrm{T}}\left(\frac{\mathbf{h}}{T}\right) \mathrm{d}t = \left(\frac{m}{T} - \beta^2 K'\right)\theta - \alpha p - \beta K' \varepsilon_v \tag{7}$$

where $\mathbf{h}^{\mathrm{T}} = (h_x, h_y, h_z)$ is the heat flux, $m = (1-n)\rho_s c_s + n\rho_w c_w$ is the heat capacity of the soil and t is the time interval considered, during which the absolute temperature increases by the amount θ to the value T. ρ_s, ρ_w and c_s, c_w are the densities and the specific heats of the soil grains and the pore water, respectively. A rate form of equation (7) is appropriate for non-linear material behaviour. The last three terms on the right-hand side of equation (7) represent the contribution from mechanical effects, which are usually very small and can often be neglected. Britto *et al.*[7] used only the first term $(m\theta/T)$ in their finite element formulation. However, the inclusion of the last three terms preserves the symmetry of the formulation. When the last three terms are small T, can be replaced by the absolute ambient temperature, T_0, without any significant loss of accuracy.

3.7. *Water flow*

It is assumed that the water flow is governed by Darcy's law, i.e.

$$\mathbf{v} = -\left(\frac{k}{\gamma_w}\right)\nabla p \tag{8}$$

where γ_w is the unit weight of water and k is the permeability of the soil which is assumed to be isotropic. However, k is assumed to be a function of temperature.

3.8. *Heat flow*

It is assumed that the heat conduction through the soil is governed by Fourier's law, i.e.

$$\mathbf{h} = -f\nabla\theta \tag{9}$$

where f is the thermal conductivity of the soil.

3.9. *Virtual work*

In the absence of any increase in body force, the equation of virtual work relating the internal strain energy to the work done by the surface tractions $\mathbf{F}$ can be written as

$$\int_V \delta\boldsymbol{\varepsilon}^{\mathrm{T}}\boldsymbol{\sigma}\,\mathrm{d}V - \int_S \delta\mathbf{u}^{\mathrm{T}}\mathbf{F}\,\mathrm{d}S = 0 \tag{10}$$

where $\delta\mathbf{u}$ represents a virtual displacement field consistent with the displacement boundary conditions and $\delta\boldsymbol{\varepsilon}$ represents the associated virtual strains.

If the boundary points are either impermeable or subjected to a specific pore pressure, and the virtual pore pressure field, δp, is consistent with these conditions, then equations (6) and (8) give

$$\int_S [\delta p v_n]\,\mathrm{d}S = \int_V \left[\delta p \frac{\partial \varepsilon_V}{\partial t} + \delta p \nabla^{\mathrm{T}}\left(\frac{-k}{\gamma_w}\nabla p\right) + \delta p \alpha \frac{\partial \theta}{\partial t}\right]\mathrm{d}V \tag{11}$$

in which v_n is the velocity of water outflow across the boundary S.

Similarly, if the boundary points are either insulated or subjected to a specified temperature, and the virtual temperature field, $\delta\theta$, is consistent with these conditions, then equations (7) and (9) yield

$$\int_S \left[\delta\theta\left(\frac{h_n}{T}\right)\right]\mathrm{d}S = \int_V \left[\delta\theta\left(K'\beta\frac{\partial \boldsymbol{\varepsilon}_v}{\partial t} + \alpha\frac{\partial p}{\partial t} - \left(\frac{m}{T} - K'\beta^2\right)\frac{\partial\theta}{\partial t} - \nabla^{\mathrm{T}}\frac{f}{T}\nabla\theta\right)\right]\mathrm{d}V \tag{12}$$

in which h_n is the heat flux across the boundary S.

3.10. Finite element formulation

A complete analysis of the fully coupled thermomechanical behaviour should include all 12 equations given above. The finite element method may be used to obtain an approximate solution to these governing equations.

Suppose that the continuous values of $\mathbf{u}, p$ and θ can be represented by their values at selected nodes, i.e.

$$\mathbf{u} = \mathbf{N}_u\boldsymbol{\delta}, \qquad p = \mathbf{N}_p\mathbf{q}, \qquad \theta = \mathbf{N}_\theta\mathbf{c} \tag{13}$$

where $\boldsymbol{\delta}, \mathbf{q}$ and $\mathbf{c}$ are the vectors containing the appropriate nodal values, and $\mathbf{N}_u, \mathbf{N}_p$ and $\mathbf{N}_\theta$ contain the shape functions of the displacements, pore pressure and temperature, respectively. The following derivatives of the shape functions are useful here:

$$\mathbf{B} = -\partial\mathbf{N}_u, \qquad \mathbf{E}_p = \nabla\mathbf{N}_p, \qquad \mathbf{E}_\theta = \nabla\mathbf{N}_q \tag{14}$$

Substituting equations (13) into equations (10)–(12) yields

$$\begin{aligned}
\mathbf{K}\boldsymbol{\delta} - \mathbf{L}^{\mathrm{T}}\mathbf{q} - \mathbf{M}^{\mathrm{T}}\mathbf{C} &= \mathbf{r}_u \\
-\mathbf{L}\frac{\mathrm{d}\boldsymbol{\delta}}{\mathrm{d}t} - \boldsymbol{\Phi}\mathbf{q} + \mathbf{Q}\frac{\mathrm{d}\mathbf{c}}{\mathrm{d}t} &= \mathbf{r}_p \\
-\mathbf{M}\frac{\mathrm{d}\boldsymbol{\delta}}{\mathrm{d}t} + \mathbf{Q}^{\mathrm{T}}\frac{\mathrm{d}\mathbf{q}}{\mathrm{d}t} - \left(\boldsymbol{\Psi}\mathbf{c} + \mathbf{X}\frac{\mathrm{d}\mathbf{c}}{\mathrm{d}t}\right) &= \mathbf{r}_\theta
\end{aligned} \tag{15}$$

where

$$\mathbf{K} = \int_V \mathbf{B}^{\mathrm{T}}\mathbf{D}\mathbf{B}\,\mathrm{d}V, \qquad \mathbf{L}^{\mathrm{T}} = \int_V \mathbf{B}^{\mathrm{T}}\mathbf{a}\mathbf{N}_p\,\mathrm{d}V$$

$$\mathbf{M}^{\mathrm{T}} = \int_V \mathbf{B}^{\mathrm{T}}K'\beta\mathbf{a}\mathbf{N}_\theta\,\mathrm{d}V, \qquad \boldsymbol{\Phi} = \int_V \mathbf{E}_p^{\mathrm{T}}\left(\frac{k}{\gamma_W}\right)\mathbf{E}_p\,\mathrm{d}V$$

$$\mathbf{Q} = \int_V \alpha\mathbf{N}_p^{\mathrm{T}}\mathbf{N}_\theta\,\mathrm{d}V, \qquad \boldsymbol{\Psi} = \int_V \mathbf{E}_\theta^{\mathrm{T}}\left(\frac{f}{T}\right)\mathbf{E}_\theta\,\mathrm{d}V$$

$$\mathbf{X} = \int_V \mathbf{N}_\theta^{\mathrm{T}}\left(\frac{m}{T} - \beta^2K'\right)\mathbf{N}_\theta\,\mathrm{d}V, \qquad \mathbf{r}_u = \int_S \mathbf{N}_u^{\mathrm{T}}\mathbf{F}\,\mathrm{d}S$$

$$\mathbf{r}_p = \int_S \mathbf{N}_p^{\mathrm{T}}\mathbf{v}_n\,\mathrm{d}S, \qquad \mathbf{r}_\theta = \int_S \mathbf{N}_\theta^{\mathrm{T}}\left(\frac{h_n}{T}\right)\mathrm{d}S$$

The solution of the set of equations (15) is obtained using a time-marching procedure. For the time interval $t - \Delta t$ to t the time integrals of $\mathbf{q}$ and $\mathbf{c}$ may be evaluated numerically, for example,

$$\int_{t-\Delta t}^{t} \mathbf{q}\, dt \approx \Delta t\, \mathbf{q}_{t-\Delta t} + \xi\, \Delta t\, \Delta \mathbf{q} \tag{16}$$

where $0 \leqslant \xi \leqslant 1$ and $\Delta \mathbf{q}$ is the change in $\mathbf{q}$ in the time interval Δt. For stability of this time-marching scheme, ξ must be greater than or equal to one-half (Reference 11). A value of 1 has been used to obtain the numerical solutions presented in this paper. The incremental solution of the set of equations (15) is then given by the system of equations

$$\begin{bmatrix} \mathbf{K} & -\mathbf{L}^{\mathrm{T}} & -\mathbf{M}^{\mathrm{T}} \\ -\mathbf{L} & -\xi\,\Delta t\,\mathbf{\Phi} & \mathbf{Q} \\ -\mathbf{M} & \mathbf{Q}^{\mathrm{T}} & -\xi\,\Delta\mathbf{\Psi} - \mathbf{X} \end{bmatrix} \begin{bmatrix} \Delta\boldsymbol{\delta} \\ \Delta\mathbf{q} \\ \Delta\mathbf{c} \end{bmatrix} = \begin{bmatrix} \mathbf{r}_u \Delta t \\ \mathbf{r}_p \Delta \mathbf{t} + \mathbf{\Phi q}\, \Delta t \\ \mathbf{r}_\theta\, \Delta t + \mathbf{\Psi c}\, \Delta t \end{bmatrix} \tag{17}$$

4. NUMERICAL MODELLING

This section describes the finite element analyses carried out to model the heat flow and pore water pressure dissipation around a long, rigid cylindrical heat source buried in clay.

4.1. Finite element program

The formulation presented in the last section has been encoded in a general finite element program called AFENA (Reference 12). The analyses were made using either the linear elastic model or the modified Cam clay model for the stress–strain behaviour. An incremental tangential stiffness formulation was used in modelling elastoplastic behaviour. Even though the program is capable of handling anisotropy in permeability and heat conductance, only isotropic properties were used in the analyses presented in this paper.

The program has the facility to allow the permeability, k, and the thermal properties, α and m, to vary with voids ratio and temperature. At any stage in the analysis the permeability is modified using the expression

$$\frac{k}{k_i} = \left(\frac{\boldsymbol{\mu}_i}{\boldsymbol{\mu}}\right)\left(\frac{e}{e_i}\right)^3 \tag{18}$$

where e and $\boldsymbol{\mu}$ are the voids ratio and the kinematic viscosity of water at time t, respectively, and e_i and $\boldsymbol{\mu}_i$ are the initial values. α and m are calculated using the expressions

$$\begin{aligned} \alpha &= \alpha_s(1-n) + \alpha_w n \\ m &= \rho_s c_s(1-n) + \rho_w c_w \mathrm{n} \end{aligned} \tag{19}$$

The kinematic viscosity, μ, and the coefficient of volume expansion of water, c_w, are linearly interpolated from a table of properties given by Chapman.[13] The accuracy of the computer code was checked exhaustively against existing solutions including the coupled elastic solutions for spherical and cylindrical heat sources given by Booker and Savvidou[4] and Smith,[3] respectively.

4.2. Idealization of the problem

The parameters of the problem were chosen to represent a real situation as close as possible. Figure 1 illustrates the configuration of the problem addressed in this paper. It shows a cylin-

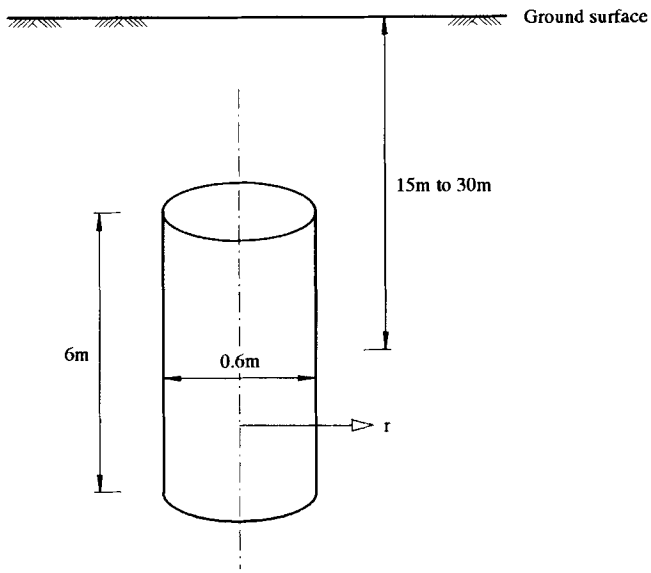

Figure 1. Typical canister embedment

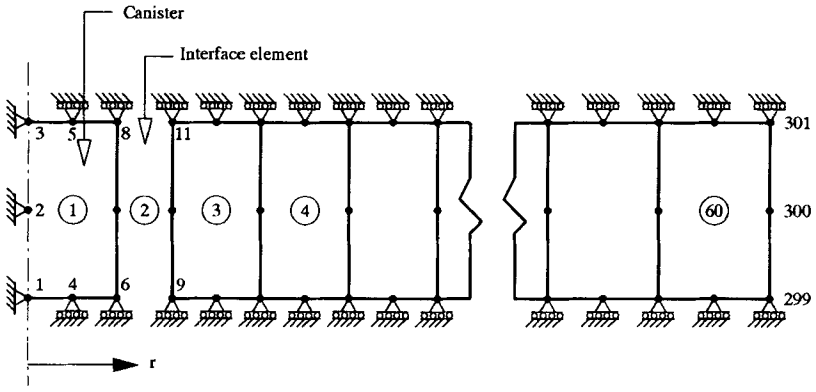

Figure 2. Finite element mesh

drical canister, typically 0·6 m in diameter, embedded vertically in an initially one-dimensionally normally consolidated soil. The canister was assumed to be nearly rigid in comparison to the surrounding soil and was assigned a large elastic stiffness. It carries a decaying radioactive source of initial power 1·8 kW with a 30 yr half-life. The finite length of the canister was not considered in the analysis and it was modelled as an infinitely long source. However, typically in practice it may be on the order of 6 m long, as indicated in Figure 1. Since the effect of gravity was also ignored there was no variation of field variables in the circumferential and vertical directions. Figure 2 illustrates the finite element mesh used for the analyses. It contains 59 eight-noded axisymmetric, isoparametric quadrilaterals, one representing the canister, 58 the soil, and one interface element. The radial length of the elements varied from 0·025 m near the canister to 48 m near the outer boundary of the soil. The height of the elements was 2 m.

The pore pressure and temperature at the boundary between the canister and the surrounding soil were unspecified. This boundary was modelled by an interface element which had the ability to separate if the radial effective stress at the interface became tensile. The pore pressure at the interface was maintained at zero after a separation occurred. However, if the inner cylindrical boundary of the soil returned to its original position, the interface element was re-established. The thermal boundary condition at the interface was not changed as a result of separation, and this assumption means that the effect of heat transfer on the surrounding soil is maximized. The outer boundary of the soil was set at a radial distance of 325 m from the centre of the canister. It was assumed to be permeable and conductive.

4.3. Finite element analyses

Three series of analyses, namely A, B and C, were carried out. A using the linear elastic soil model and the other two using the modified Cam clay stress–strain model. In all the analyses, initially the soil was assumed to be one-dimensionally normally consolidated with an effective vertical stress, σ'_{vi} equal to 300 kPa and a coefficient of earth pressure at rest, K_{nc} equal to 0·69. This initial stress state represents a depth of embedment in the range from 15 to 30 m, depending on the position of the watertable. In the series A and B, it was assumed that the emplacement of the canister did not disturb the soil around it. In the series C, it was assumed that a borehole was excavated prior to the placement of the canister; the excavation phase was modelled as cavity unloading using a time period of 1000 s. The excess pore pressure at the cavity boundary was assumed to be zero during the cavity unloading. Thereafter, the canister was assumed to be placed in the borehole without further disturbance and delay, and the internal boundary was assumed to be impermeable unless separation occurred. In all other aspects the series C was the same as the series B. Separation at the interface between the canister and the surrounding soil was allowed only in the series B and C analyses.

Three analyses with different initial soil permeabilities were carried out in each series. The initial values assumed for the coefficient of permeability were $2{\cdot}5 \times 10^{-9}$, $2{\cdot}5 \times 10^{-10}$ and $5{\cdot}0 \times 10^{-11}$ m/s. The value of $2{\cdot}5 \times 10^{-9}$ m/s might be considered somewhat high for a waste disposal site, but it is consistent with the value adopted by Britto *et al.*[8] for kaolin in their centrifuge and analytical studies. In the series A, none of the material properties was allowed to vary from the initial values. In contrast, in the series B and C, the permeability, k, the coefficient of undrained thermal volume expansion, α, and the thermal capacity of the soil, m, were allowed to vary with temperature and voids ratio according to expressions (18) and (19).

4.4. Material properties

The initial pore pressure in the soil prior to the emplacement of the canister was assumed to be zero. The initial temperature of the soil was assumed to be 300 K. The material properties used in the elastic analyses (series A) are given in Table I. The elastic bulk modulus of the soil, K', was calculated from the elastic properties of the initially normally consolidated soil using the expressions

$$K' = \frac{p'(1+e)}{\kappa}, \qquad p' = \frac{\sigma'_{vi}(1+2K_{nc})}{3}. \tag{20}$$

The coefficient of undrained thermal expansion, α, was calculated using expression (19) and an absolute temperature of 333 K. The thermal capacity of the soil was calculated using expression (19) and the initial voids ratio.

Table I. Parameters for the elastic analyses

Parameter	Units	Value
K'	kPa	10358
ν'	Dimensionless	0·25
α	/°C	$2{\cdot}982 \times 10^{-4}$
β	/°C	$-5{\cdot}0 \times 10^{-4}$
K_{nc}	Dimensionless	0·69
m	kJ/m³/°C	3386
$k = k_i$	m/s	$2{\cdot}5 \times 10^{-9}$
		$2{\cdot}5 \times 10^{-10}$
		$5{\cdot}0 \times 10^{-11}$
γ_w	kN/m³	9·81
f	kW/m/°C	$1{\cdot}5 \times 10^{-3}$
T_0	°K	300

Table II. Parameters for the modified Cam clay analyses

Parameter	Units	Value
M	Dimensionless	0·90
λ	Dimensionless	0·25
κ	Dimensionless	0·05
e_{cs}	Dimensionless	2·44
ν'	Dimensionless	0·25
α	/°C	equation (19)
α_s	/°C	$3{\cdot}5 \times 10^{-5}$
α_w	/°C	Tables by Chapman[13]
β	/°C	$-5{\cdot}0 \times 10^{-4}$
k	m/s	equation (18)
$k = k_i$	m/s	$2{\cdot}5 \times 10^{-9}$
		$2{\cdot}5 \times 10^{-10}$
		$5{\cdot}0 \times 10^{-11}$
m	kJ/m³/°C	equation (19)
c_s	kJ/kg/°C	0·937
c_w	kJ/kg/°C	4·186
ρ_s	kg/m³	2610
ρ_w	kg/m³	1000
γ_w	kN/m³	9·81
f	kW/m/°C	$1{\cdot}5 \times 10^{-3}$
K_{nc}	Dimensionless	0·69
T_0	°K	300

The parameter values for the modified Cam clay model are given in Table II. Most of them are taken from the values for kaolin used by Britto *et al.*[8] in their analyses of soil heating. One exception is the value of β; a higher value of β has been used in the present work, as the value used by Britto *et al.* appears to be low in comparison to the data on other soils (Reference 14). The analyses were carried out with a constant value of β, although the experiments have shown that β may decrease with the degree of overconsolidation (Reference 14). Unlike the analyses carried out by Britto *et al.*,[8] in the analyses described here α, m and k were allowed to vary with the temperature and voids ratio.

5. NUMERICAL RESULTS

The results of the series A, B and C finite element analyses are discussed in this section. Predictions of the nodal values of displacement, temperature and pore pressure, and the stresses at the centroid of the elements are presented graphically in Figures 3–19. The stresses and pore pressure have been normalized by the initial vertical effective stress, $\sigma'_{vi} = 300$ kPa. The displacements have been normalized by the radius of the canister, b. The time after canister emplacement, t, has been normalized using a time factor, T, given by

$$T = \frac{k't}{b^2} \tag{20}$$

where k' is the thermal diffusivity of the soil given by

$$k' = \frac{f}{m} \tag{21}$$

Since k' varies in the modified Cam clay analyses due to change in voids ratio, its initial value before canister emplacement was used for the normalization. In the three analyses performed in each series, the ratio c_v/k' (c_v is the coefficient of consolidation) was based on the initial elastic properties of the soil, so that $c_v/k' = 10{\cdot}73$, $1{\cdot}07$ and $0{\cdot}21$, respectively.

5.1. *Temperature distribution*

Figure 3 illustrates the isochrones of temperature in the analysis A2, i.e. the linear elastic analysis with $k = 2{\cdot}5 \times 10^{-10}$ m/s. The predicted maximum temperature is at the canister surface and occurs at a time factor of 950, i.e. a period of 7·9 yr after the canister emplacement. The initial rise in the temperature at any point is much slower than the rate of decrease in the temperature

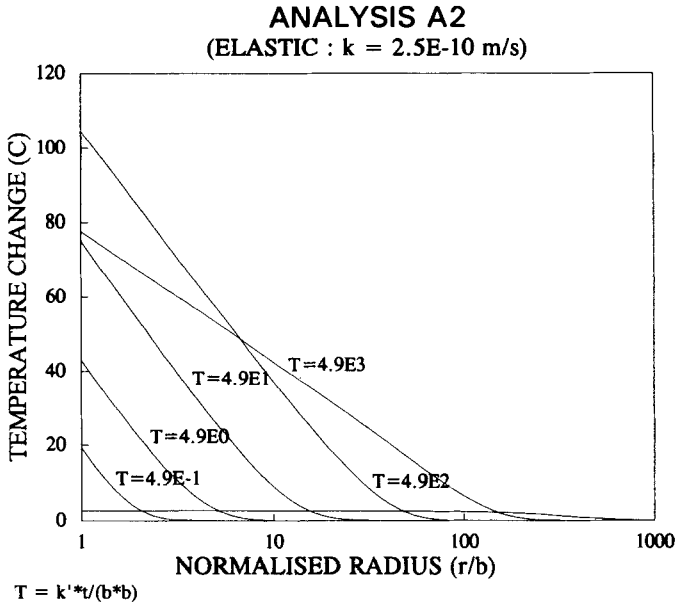

Figure 3. Isochrones of temperature change – case A2

towards the end of cooling. The differences in the temperature distribution in the linear elastic analyses and modified Cam clay analyses were insignificant. This is due to negligible contribution from mechanical terms to the heat equation (7), and also due to the relative insensitivity of the thermal capacity of the soil to changes in voids ratio.

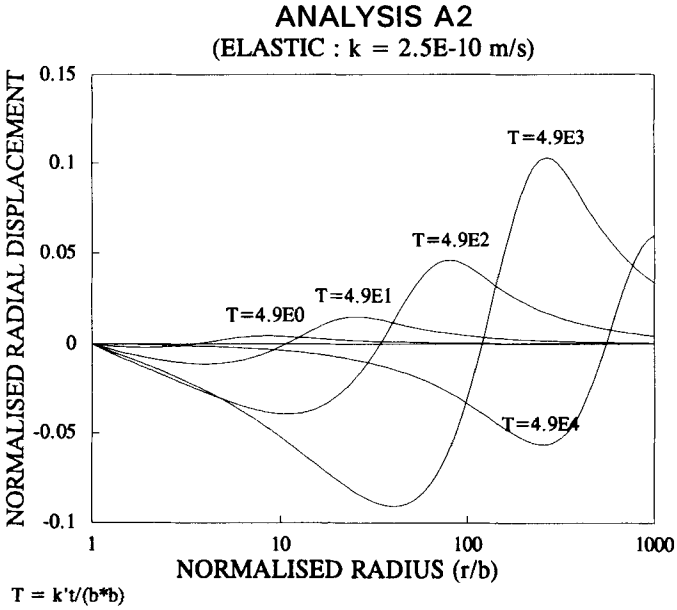

Figure 4. Isochrones of radial displacement – case A2

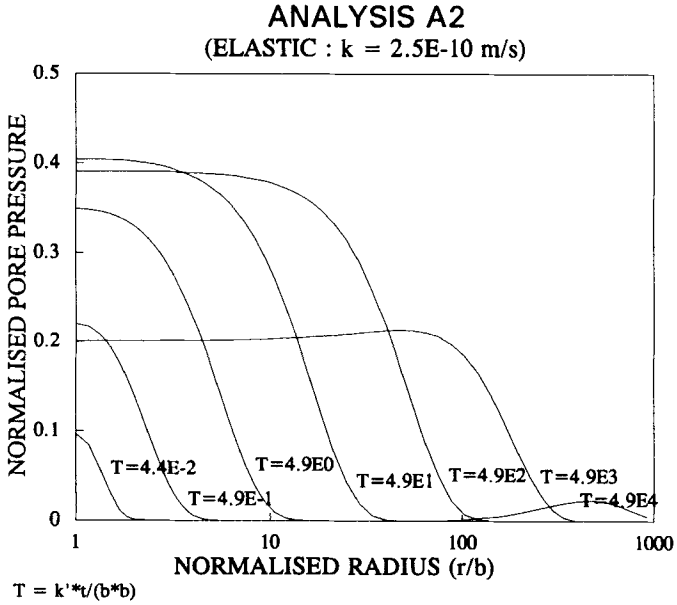

Figure 5. Isochrones of pore pressure – case A2

5.2. Linear elastic analyses

Figure 4 illustrates the isochrones of radial displacement in the analysis A2. There is no radial displacement at the canister since it was specified as zero in this case. The displacement distribution is characterized by radial expansion at large distances and by radial contraction close to the canister. Figure 4 clearly shows the advancement of expansive and contractive fronts with time. Similar behaviour was also observed in the analyses A1 ($k = 2{\cdot}5 \times 10^{-9}$ m/s) and A3

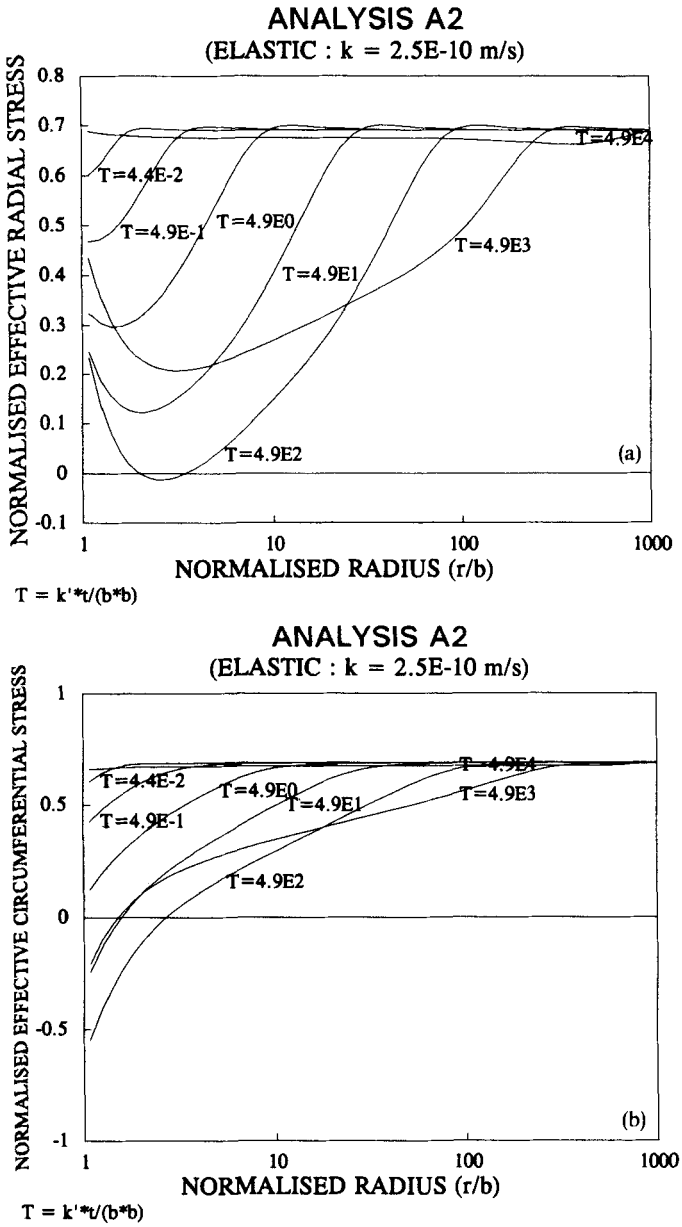

Figure 6. Isochrones of stress components – case A2

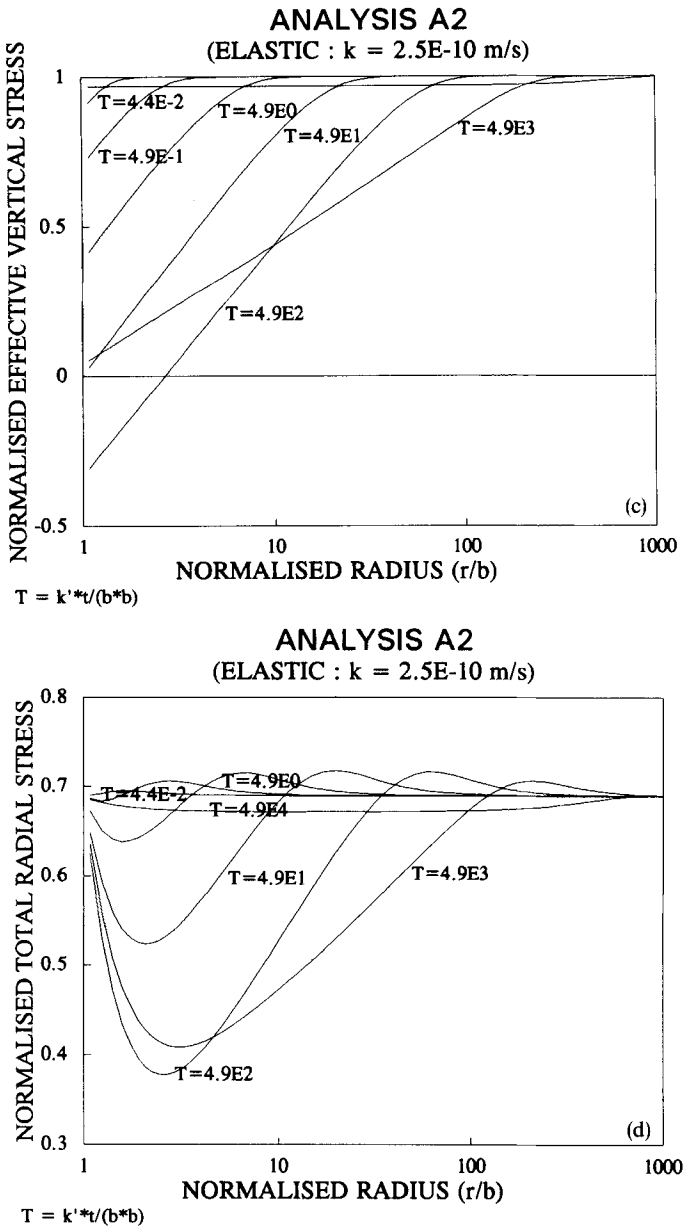

Figure 6 continued

($k = 5{\cdot}0 \times 10^{-11}$ m/s). The reason for these rather unusual contractive strains is the magnitude of β used in the analyses. A smaller value of β may not produce such contractive behaviour. The maximum values of contractive and expansive radial strains in all the analyses were substantial, in the order of 10–15%. The main differences in the displacement predictions in the three analyses were that in the more permeable cases the maximum radial expansion was reduced, the maximum

radial contraction was increased, and the advance of the contraction front was quicker than in the less permeable soils.

Figure 5 illustrates the isochrones of excess pore pressure in the analysis A2. Significant pore pressures were generated even at large distances ($r/b > 100$) away from the canister. Like the temperature distribution, the rate of rise in the pore pressure was much slower than the rate of dissipation. The maximum pore pressure at a point occurs before the maximum temperature. Significant pore pressures remain even after the half-life period of the radioactive heat source has expired. The characteristics of the distribution of pore pressures found in the analyses A1 and A3 were also similar to those described above. However, the magnitude of maximum pore pressure was much larger in the less permeable soil.

Figures 6(a)–6(c) illustrate the isochrones of effective normal stresses in the analysis A2 in the radial, circumferential and vertical directions, respectively. The distributions of circumferential and vertical stress are similar and show the occurrence of tensile stresses in the vicinity of the canister in the middle period of heat dissipation; both illustrate stresses monotonically increasing away from the canister. The effective radial normal stress also became negative at some distance away from the canister. However, the maximum tensile stress occurs in the circumferential direction.

Figure 6(d) shows the isochrones of total radial stress obtained in the analysis A2. At the canister no increase in total radial stress (above the initial value of 0·69 σ'_{vi}) is predicted. This interesting behaviour confirms the independent theoretical solution for the same problem given by Smith.[5]

Figure 7 illustrates the effective stress paths in deviator (q)—mean effective stress (p') space of four points situated at radial distances defined by r/b = 1·25, 2·42, 4·87 and 9·95. For comparison purposes, the modified Cam clay yield locus corresponding to the initial *in situ* stress state and the critical state line are also shown in Figure 7. It is interesting to see the difference in stress paths of points close to the canister and those well away from it. The stress paths of points close to the

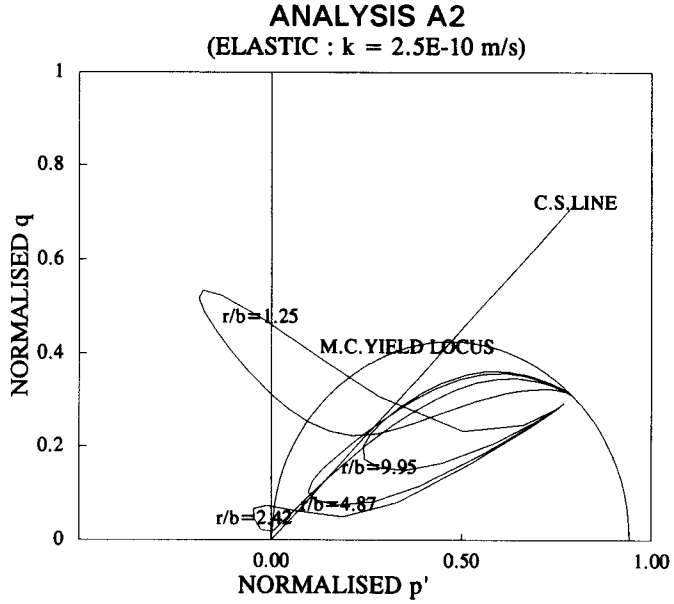

Figure 7. Effective stress paths – case A2

canister show a general increase in the deviator stress with a decrease in the mean normal stress towards the middle period. Further from the canister, the stress path involves an overall reduction in both the deviator stress and the mean stress during the middle period. However, the figure also indicates that the states of stress at all points return to the original condition at large

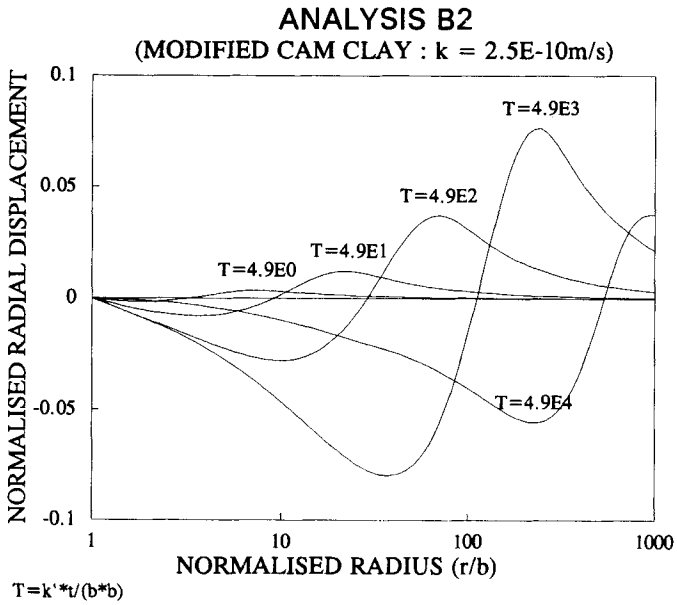

Figure 8. Isochrones of radial displacement – case B2

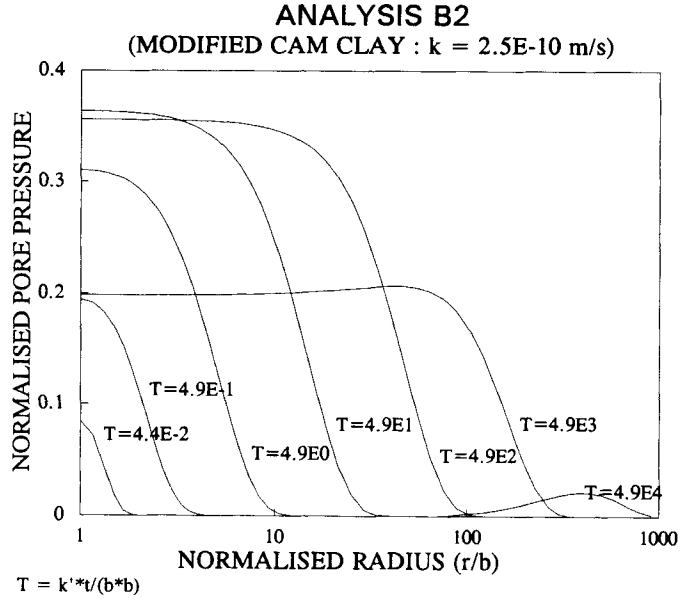

Figure 9. Isochrones of pore pressure – case B2

times, at the end of heating and consolidation. This is to be expected for a linear elastic soil. Similar behaviour was also observed in the other two elastic analyses, A1 and A3. The main difference between the analyses is that the intermediate changes in stresses near the canister are greater in less permeable soils. The separation between the soil and the canister, had it been allowed, could have occurred only in the analysis A3 in which the permeability of the soil was the lowest ($k = 5 \times 10^{-11}$ m/s). However, the results of all the analyses suggest that fracture could have occurred in the soil close to the canister where the effective stresses were predicted to be negative.

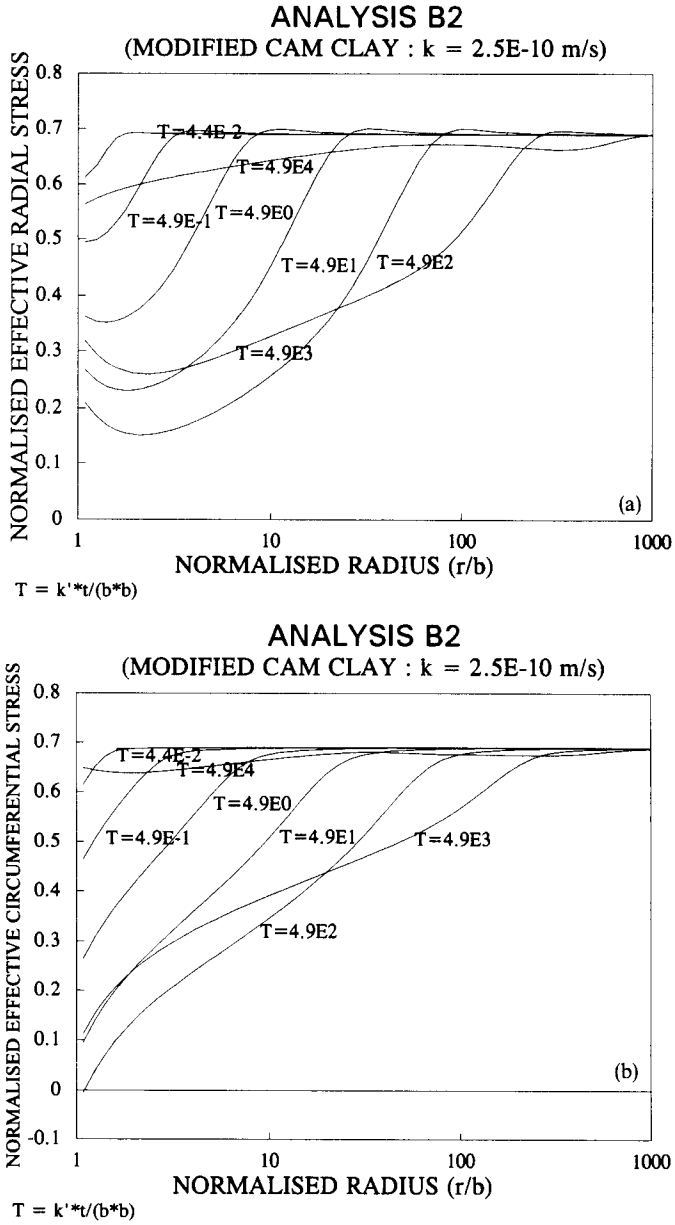

Figure 10. Isochrones of stress components – case B2

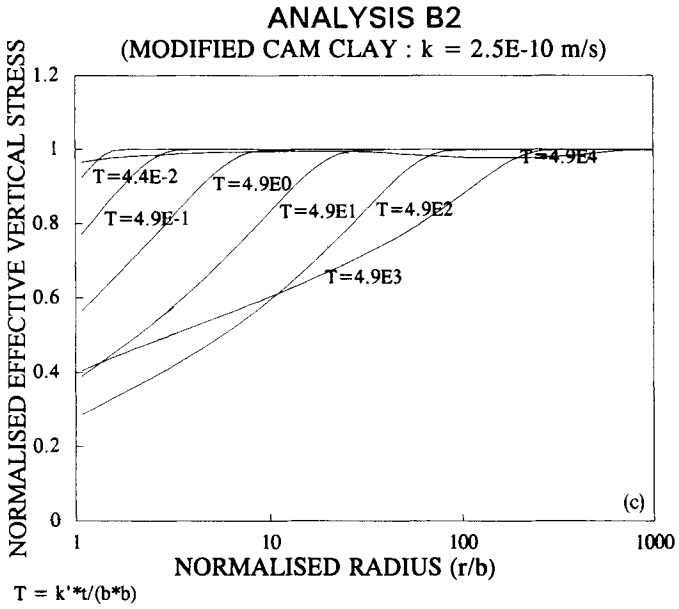

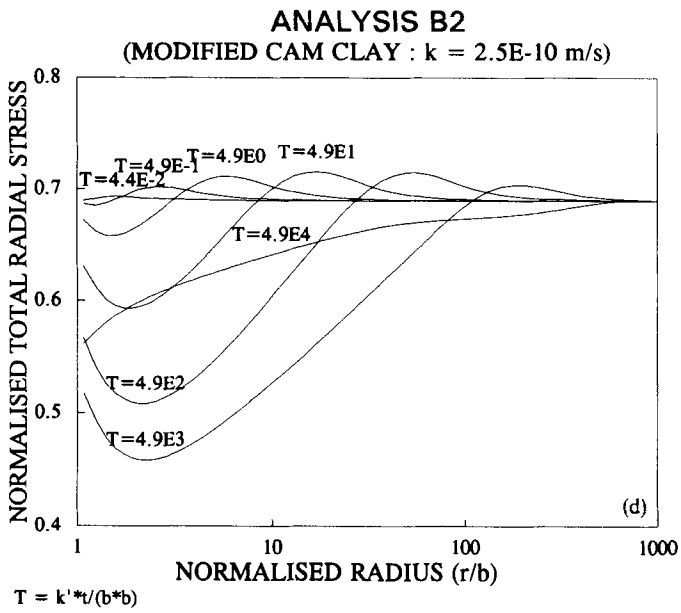

Figure 10 continued

5.3. *Modified Cam clay analyses—series B*

Figures 8 and 9 illustrate the isochrones of radial displacement and pore pressure in the analysis B2 in which the initial soil permeability was $2{\cdot}5 \times 10^{-10}$ m/s. The distributions of radial, circumferential and vertical effective stresses and total radial stress in the same analysis are shown in the Figures 10(a)–10(d). The various distributions are basically similar to their counterparts in

the linear elastic analysis A2, but there are differences in the stress magnitudes (cf. Figures 10(a)–10(d) and 6(a)–6(d). Even though very little yielding occurred in the analysis B2, there are significant differences in the stresses predicted at very large times in the analyses B2 and A2. Since the material behaviour in both cases was predominantly elastic, this shows the inadequacy of using constant values for properties like k and α (as in case A2), when these parameters are actually functions of temperature and voids ratio (as assumed in case B2).

Figure 11 illustrates the effective stress paths of points at radial positions given by r/b = 1·25, 2·42, 4·87 and 9·95. Most of the soil follows paths that lie largely inside the initial yield locus, indicating predominantly elastic behaviour for this case. While the last two points, which are well away from the canister, follow stress paths similar to those observed in the linear elastic analysis, this is not the case with the points closer to the canister (cf. Figures 7 and 11). Unlike the linear elastic case, in the analysis B2 no increase in the deviator stress occurred simultaneously with a reduction of mean normal effective stress close to the canister. Furthermore, the mean effective stress was always compressive in the non-linear analysis. In general, the change in deviator stress at intermediate times during heat dissipation was smaller in the modified Cam clay analysis than in the case of a linear elastic soil.

Figure 12 illustrates the variations with time of total pressure, effective pressure and pore pressure on the canister and the temperature at the canister boundary. The change in total pressure on the canister during heat dissipation is not large, with a maximum of 22·5% reduction over the initial pressure. The pore pressure at the canister reaches a maximum value well before the occurrence of the peak temperature, at a time of 0·8 years after the canister emplacement. Unlike the linear elastic analysis, in the analysis, B2 the effective stresses never became tensile and hence no separation occurred.

Similar behaviour to that described above was also found in the analyses B1 and B3. No separation occurred in any of the three analyses and the effective stresses were compressive

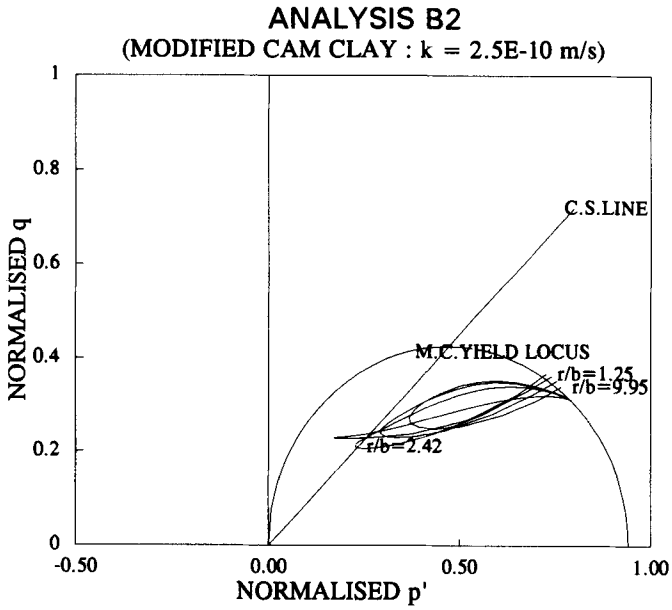

Figure 11. Effective stress paths – case B2

everywhere throughout the heat dissipation. Except in the analysis B3, in which a maximum of 3% increase over the initial pressure occurred, the pressure on the canister was always below the initial pressure. The stress paths in the analysis B3 were similar to those in the analysis B2. In contrast, the stress paths in the analysis B1 were similar in shape to the linear elastic stress paths.

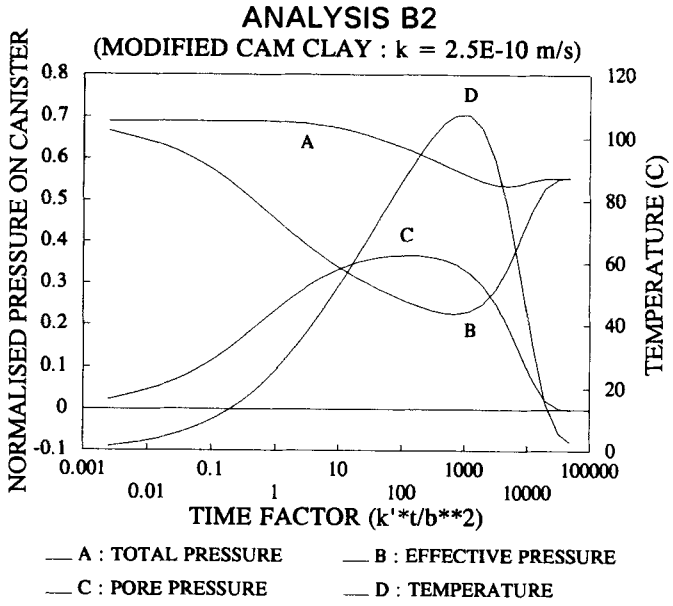

Figure 12. Temporal variations of pressure and temperature at the canister – case B2

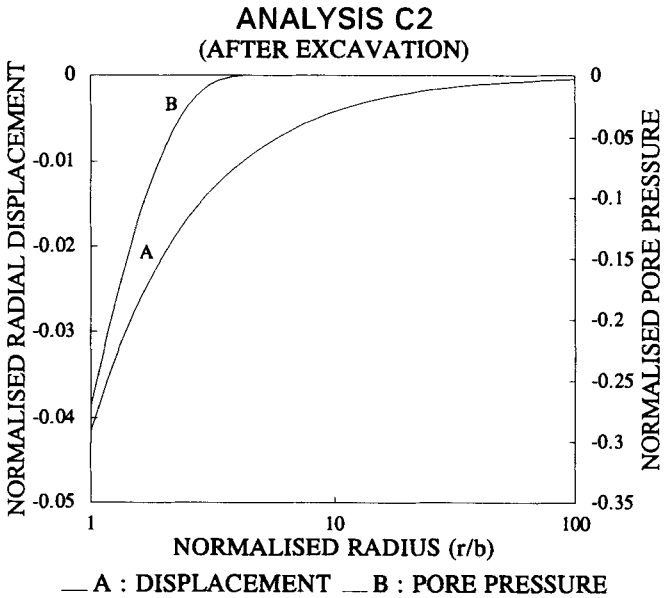

Figure 13. Displacement and pore pressure after excavation – case C2

Some numerical instability was encountered with the solution at some distance away from the canister during the analysis B3. The exact reason for the instability is not clear; however the complexity of the stress path which traverses close to the critical state into the softening region may be a factor contributing to this numerical instability. It is well known that the modified Cam clay model does not perform well in this region of stress space.

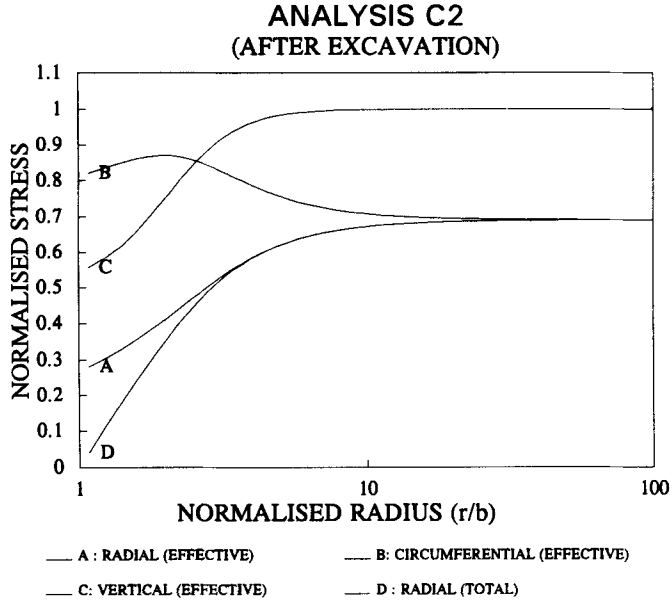

Figure 14. Stress components after excavation – case C2

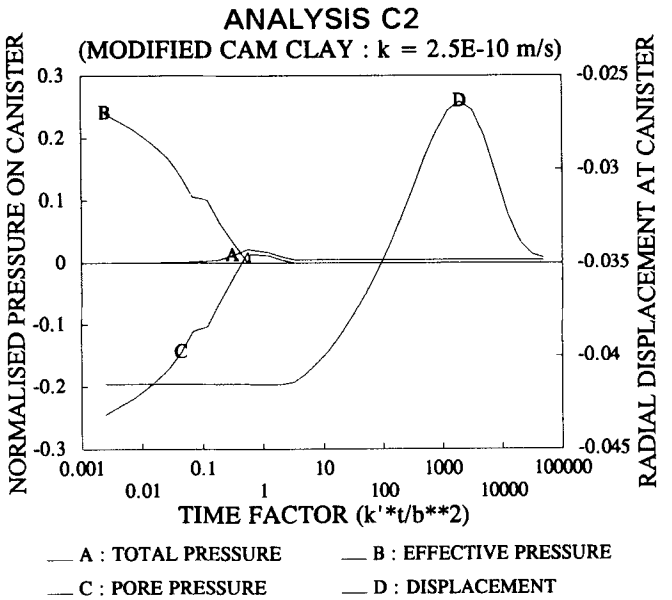

Figure 15. Temporal variations of pressure and temperature at the canister – case C2

5.4. Modified Cam clay analyses – series C

Figure 13 illustrates the distribution of radial displacement and pore pressure due to simulated excavation of a borehole prior to canister emplacement in the analysis C2 ($k = 2{\cdot}5 \times 10^{-10}$ m/s). The distributions of radial, circumferential and vertical effective stress and the total radial stress at the same stage are shown in Figure 14. During the small excavation period (1000 s), very little

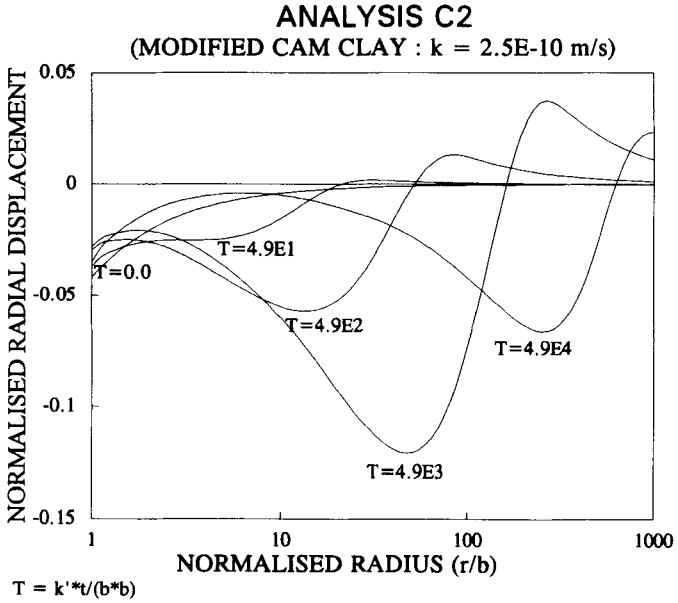

Figure 16. Isochrones of radial displacement – case C2

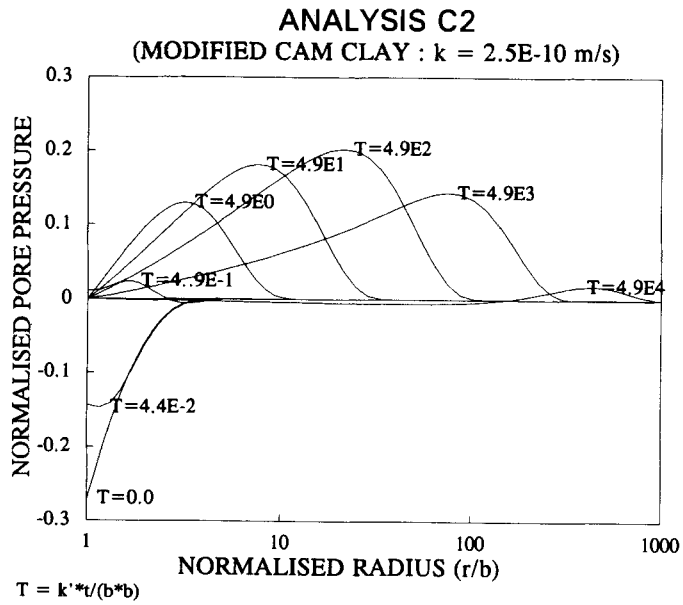

Figure 17. Isochrones of pore pressure – case C2

drainage occurred and the soil behaviour was almost completely undrained; the pore pressures remained negative and the effective stresses near the hole were compressive even after the complete removal of the lateral pressure at the borehole. Failure occurred near the borehole with a few elements reaching the critical state, however, no numerical problems were encountered.

Figure 15 illustrates the variation with time of the stresses and normal displacement at the interface between the canister and the surrounding soil. A separation occurred at the interface at a time factor of 0·6 (half a day after the canister emplacement). The relative displacement at the

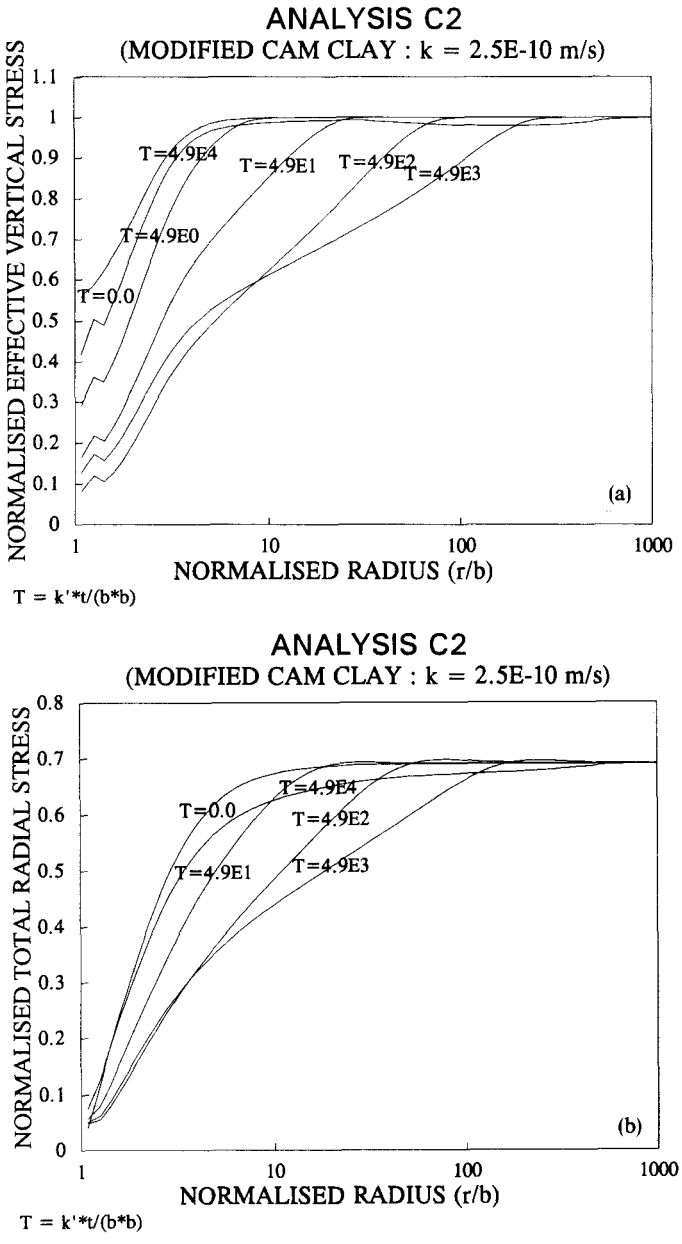

Figure 18. Isochrones of stress components – case C2

interface increased initially after the separation but decreased at large times, although the contact was never re-established. After the separation the pore pressure at the canister boundary was specified as zero and drainage towards the canister was then permitted. The total pressure on the canister was zero except in the period immediately before and after separation during which time a small radial pressure developed at the interface.

Figures 16 and 17 illustrate the isochrones of radial displacement and pore pressure, respectively, during heat dissipation in the analysis C2. The isochrones of effective and total radial stress and the stress paths followed by some selected points in the same analysis are shown in Figures 18(a)–18(b) and 19, respectively. The values shown in the above figures include the effect of borehole excavation. In the analyses B2 and C2, in the areas away from the canister ($r/a > 3$), the displacement distributions due to heat dissipation are similar (cf. Figures 16 and 8). However, even in these areas the magnitudes of the radial displacements differ substantially in the two analyses. In comparison to the case B2, in the analysis C2 the maximum pore pressure at any point is considerably smaller and the rate of consolidation higher (cf. Figures 17 and 9). This is due to the drainage towards the canister after the separation. The distributions of total and effective radial stresses in the two analyses are also different. The stress paths of points in the vicinity of the canister in the analysis C2 (Figure 19) show a horizontal trajectory towards the critical state line followed by unloading almost parallel to the critical state line. The soil behaviour in the analysis C2 during heat dissipation was mainly elastic with a little yielding, and the stress paths for this period indicated a general increase in both deviator and mean effective stress. The contrasting behaviour in the two analyses C2 and B2 in the vicinity of the canister is due to two reasons, namely, the effect of borehole excavation and the occurrence of separation in case C2.

The modified Cam clay yield locus drawn in Figure 19 corresponds to the *in situ* stress state prior to canister emplacement. In Figure 19 some of the paths describe elastic behaviour, but close to the canister (e.g. $r/b = 1{\cdot}25$) the stress state involves some initial hardening and move-

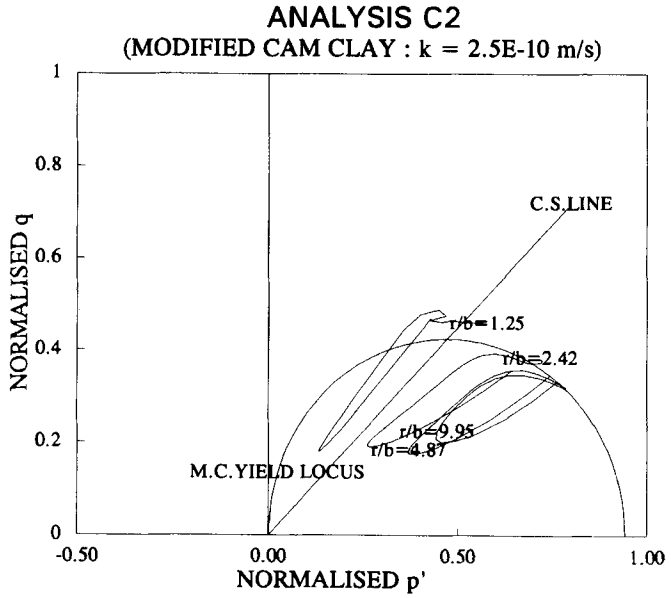

Figure 19. Effective stress paths – case C2

ment onto the 'dry' side of critical state during cavity creation, followed by elastic unloading and reloading with heating and cooling, as mentioned previously.

The behaviour in the analyses C1 was similar to that in the analysis C2 described above. However, numerical problems manifesting themselves as ripples in the stress distributions occurred in the analysis C3, and therefore the results of this analysis are considered unreliable.

6. CONCLUDING REMARKS

The following conclusions may be drawn from the numerical results of the analyses presented in this paper.

1. The temperature and pore pressure generated after a canister emplacement may be substantial and may propagate to considerable distances over a long period. However, the peak values may be less and the consolidation and heat dissipation may be quicker if the finite length of the canister is considered. Smaller peak pore pressures are predicted in more permeable soils. The temperature distribution is virtually independent of the mechanical behaviour of the soil, illustrating the negligible contribution from the mechanical terms to heat transfer.
2. The selection of reasonable material properties for linear elastic analyses is difficult. However, an elastic analysis which incorporates the correct variation of properties with the temperature and voids ratio and allows tensile fracture may give results similar to a more sophisticated modified Cam clay analysis.
3. Separation of the surrounding soil from the canister may not occur in cases where the canister is placed without much disturbance. It is difficult to model the exact manner in which a soil may get disturbed during the canister emplacement. However, the analyses presented here illustrate that a decrease in effective radial stress near the canister during emplacement may increase the possibility of separation. It is difficult to assess the possible damage due to a separation, as the behaviour subsequent to a separation is likely to be very complicated. There may be some beneficial effects as well, with the flow of water towards the canister after a separation reducing the outward migration of potentially contaminated pore fluid, and also accelerating the heat and pore pressure dissipation, thus reducing the tensile stresses.
4. The total pressure on the canister seems to be not significantly larger than the *in situ* soil pressure in all the cases examined.
5. The analyses presented here were carried out with a constant value for the coefficient of effective thermal volume expansion of the soil, β. However, β is known to vary with the degree of overconsolidation and also possibly with the stress ratio. Since the stress paths of the points close to the canister show large variation in the stress ratio and the degree of overconsolidation, the analyses presented here could be improved by using a suitable variation of β.

Finally, the predictions presented here are based on a limited understanding of the fundamental thermomechanical behaviour of clays that is available at present in the literature. These results should be verified in a laboratory or a field situation before they can be applied confidently. More research, experimental as well as analytical, on the fundamental thermomechanical behaviour of soils, particularly thermal behaviour under deviatoric stresses, tensile fracture, and thermomechanical stress–strain models, is necessary for further progress in this field.

ACKNOWLEDGEMENTS

This work forms part of a research project investigating the thermomechanical behaviour of soil and rock. This work is supported by a grant from the Australian Research Council.

NOTATION

$\mathbf{a}$	vector $(1, 1, 1, 0, 0, 0)^T$
b	outer radius of the canister
c_s	specific heat of soil grains
c_v	coefficient of consolidation
c_w	specific heat of pore water
$\mathbf{D}$	matrix of elastoplastic parameters
e	voids ratio
e_{cs}	voids ratio at unit pressure on the critical state line
f	thermal conductivity
G	shear modulus
$\mathbf{h}$	vector of heat flux
k	coefficient of permeability
k_i	initial coefficient of permeability
k'	thermal diffusivity of soil
K'	effective bulk modulus
K_{nc}	Coefficient of lateral earth pressure (1-D normally consolidated soil)
m	heat capacity
n	porosity
p	excess pore pressure
p'	effective pressure
q	octahedral deviator stress
$\mathbf{q}$	vector of excess pore pressures
r	radial distance from the centre of the canister
t	time interval
T	time factor $(k't/b^2)$ or absolute current temperature
T_0	absolute ambient temperature
$\mathbf{u}$	vector of displacement components
$\mathbf{v}$	seepage velocity vector
α	coefficient of undrained thermal volume expansion
α_s	coefficient of volume expansion of soil grains
α_w	coefficient of volume expansion of pore water
β	coefficient of effective thermal volume expansion
γ	engineering shear strain
γ_w	unit weight of water
$\boldsymbol{\varepsilon}$	vector of strain components
ε_v	volumetric strain
θ	temperature increase
k	gradient of swelling line in e–ln p' space
λ	gradient of normally consolidation line in e–ln p' space, modified Cam clay
λ	Lamé parameter, elastic soil model
μ	kinematic viscosity of water
M	gradient of critical state line

ν' effective Poisson ratio
ρ_s density of soil grains
ρ_w density of pore water
$\boldsymbol{\sigma}$ vector of total stress increments
$\boldsymbol{\sigma}'$ vector of effective stress increments
σ'_{vi} initial vertical effective stress

REFERENCES

1. R. A. Forsch, 'Disposing of high-level radioactive waste', *Oceanus*, **20**(1), 5–17 (1977).
2. C. E. Hickox and H. A. Watts, 'Steady thermal convection from a concentrated source in a porous medium', *Trans. ASME*, **102**, 248–253 (1980).
3. L. M. Wickens, 'The pore-water and effective stress response of clay sediments to a heat source', *Report TP. 966*, Theoretical Physics Division, AERE Harwell, Oxon. OX11 ORA.
4. J. R. Booker and C. Savvidou, 'Consolidation around a point heat source', *Int. j. numer anal. methods geomech.*, **9**(2), 173–184 (1985).
5. D. Smith, 'Boundary element analysis of heat flow and consolidation for geotechnical applications', *Ph.D. Thesis*, University of Sydney, 1990.
6. R. W. Lewis, C. E. Majorana and B. A. Schrefler, 'A coupled finite element model for consolidation of non-isothermal media', *Transport in Porous Media*, **1**, 155–178 (1986).
7. A. M. Britto, C. Savvidou, M. J. Gunn and J. R. Booker, 'Finite element analysis of the coupled heat flow and consolidation around hot buried objects', *Soil Foundations*, submitted.
8. A. M. Britto, C. Savvidou, D. V. Maddocks, M. J. Gunn and J. R.Booker, 'Numerical and centrifuge modelling of coupled heat flow and consolidation around hot cylinders buried in clay', *Géotechnique*, **39**(1), 13–25 (1989).
9. T. Hueckel, M. Borsetto and A. Peano, 'A study of thermo-plastic–hydraulic coupling in clays applied to nuclear waste disposal', *Proc. 2n Int. Conf. on 'Constitutive Laws for Engineering Materials: Theory and Application'*, Vol. 1, Tucson, AZ, 1987, pp. 311–318.
10. A. M. Britto and M. J. Gunn, *Critical State Soil Mechanics via Finite Elements*, Ellis Horwood, Chichester, 1987.
11. J. R. Booker and J. C. Small, 'An investigation of the stability of numerical solutions of Biot's equations of consolidation', *Int. j. solids struct.* **11**, 907–917 (1975).
12. J. P. Carter and N. P. Balaam, *A Finite Element Numerical Algorithm – Users' Manual*, School of Civil and Mining Engineering, University of Sydney, Australia, 1990.
13. A. J. Chapman, *Heat transfer*, Macmillan, New York, 1967.
14. H. N. Seneviratne, J. P. Carter, D. W. Airey and J. R. Booker, 'A review of models for predicting the thermo-mechanical behaviour of soft clays', *Int. j. numer. anal. methods geomech.*, **17**, 715–733 (1993).